RSC Advances

PAPER

View Article Online
View Journal | View Issue

Cite this: *RSC Adv.*, 2020, **10**, 5853

A novel cerium(III)–isatin Schiff base complex: spectrofluorometric and DFT studies and application as a kidney biomarker for ultrasensitive detection of human creatinine†

Sheta M. Sheta, *[a] Magda A. Akl,[b] Heba E. Saad[b] and El-Sayed R. H. El-Gharkawy[b]

In this paper, a new isatin-Schiff base **L1** was prepared *via* a simple reaction of isatin with 2-amino-3-hydroxypyridin. Subsequently, cerium(III)-Schiff base complex **C1** was obtained through the reaction of the prepared Schiff base **L1** with cerium chloride *via* a hydrothermal method. The prepared **L1**, as well as **C1**, were fully characterized using many spectroscopic techniques, such as mass spectra, elemental analysis, UV-vis, FT-IR, ^{1}H-NMR, ^{13}C-NMR, FE-SEM/EDX, and HR-TEM. A photoluminescence study (PL) was carried out for the prepared complex **C1**. The promising photoluminescence results revealed that **C1** could be used for the detection of creatinine in different human biological samples as a selective optical biosensor. The results showed that **C1** after excitation at 370 nm has a strong emission band at 560 nm. The calibration graph was obtained in a wide concentration range between 2.5 and 480 nM creatinine with limits of detection (LOD) and quantitation (LOQ) of 1.07 and 3.25 nM, respectively. In addition, the correlation coefficient (r^2) was found to be 0.9890. The PL spectra indicate that **C1** has high selectivity toward creatinine without interference from other different analytes and can be successfully used as an optical sensor for creatinine detection. The mechanism of quenching between the Ce(III) complex and creatinine was a dynamic type. The geometry of Schiff base **L1** and its cerium(III) complex **C1** was proven by using density functional theory (DFT). The energy of the LUMO and HOMO, energy gap, dipole moment and structure–activity relationship were determined and confirmed.

Received 3rd December 2019
Accepted 20th January 2020

DOI: 10.1039/c9ra10133k

rsc.li/rsc-advances

Introduction

Cerium complexes have a wide range of applications in miscellaneous fields because of their significant electromagnetic properties.[1] These complexes have an excessive influence in the fields of optics, physics, and engineering.[1] They can be used as electroluminescence devices[2] and bio-makers,[3] they are imperative for the fabrication of optical waveguides[4] and metamaterials, and they possess numerous applications, such as in antenna,[5] photo-detection,[6] light-emitting diodes, laser diodes and cloaking devices.[7,8] Organic Ce(III) complexes are recognized to emit in the UV to green region, between 300 and 550 nm, with their emission wavelength being tunable through selection of appropriate ligands.[8,9] Benefited by such tunability, the above complexes can be used as light sources. This is a protuberant characteristic of Ce(III) complexes in contrast to conservative complexes of lanthanides, such as Eu(III) and Tb(III), which emit in the green and orange region, correspondingly, due to their 4f–4f transitions.[10]

Compared to complexes of lanthanides that display a 4f–4f transition,[10] the spin allowed 4f–5d transitions in the Ce(III) complexes are predicted to result in enormous emission quantum yields (Φ_{em}), as well as a short emission lifetime (τ_{em}). Also, if the complexes with 4f–4f transitions work as an emitter, a suitable ligand structure must be selected. In practice, the modification of the structures of the ligands, such as the substitution of C–H bonds with C–D and C–F bonds, can be carried out to gain great Φ_{em} values.[11] In contrast, Ce(III) complexes are approximately free from such limitations in the selection of ligands. One of the small restrictions of these species is that the coordination of solvents with hydroxyl-functionalities to Ce(III) may modify the structure of the complex, which should be avoided.[12]

On the other hand, Schiff bases create a significant category of organic compounds with an extensive range of biological properties, including cytotoxic, anticancer, and antifungal activities.[13–15] Different derivatives of isatin are known to have an extensive variety of pharmacological properties.[16] Among those paramount pharmacological effects are antibacterial,[17] antifungal,[8] antiviral[18] and anti-HIV[17] activity.

[a]*Inorganic Chemistry Department, National Research Centre, 33, El-Behouth St., Dokki, Giza, 12622, Egypt. E-mail: dr.sheta.nrc@gmail.com; Fax: +20-2-33370931; Tel: +20-1009697356*

[b]*Chemistry Department, Faculty of Science, Mansoura University, Mansoura, Dakahlia, 35516, Egypt*

† Electronic supplementary information (ESI) available. See DOI: 10.1039/c9ra10133k

Creatine (2-amino-1-methyl-5*H*-imidazol-4-one)[19] is metabolized into creatinine in tissues and organs, and adenosine triphosphate is known to take part in this conversion. Before this step, creatine is synthesized mainly in the pancreas, liver, and kidneys.[20] Creatinine is a chemical waste product of normal muscle function in the blood that passes through the kidneys to be purified and removed in the urine. The levels of creatinine in the blood reflect both the amount of muscle a person has and their amount of kidney function.[21] Around 95% of the creatine in the human body is stored in skeletal muscle and 5% is in the brain, so it is a source of energy for muscle activity and the brain.[22] Most men with normal kidney function have approximately 60 to 110 μM of creatinine and women with normal kidney function have between 45 and 90 μM of creatinine. Serum creatinine allows us to dictate the glomerular filtration rate (GFR).[23] Creatinine clearance (Ccr) measures how well the kidneys filter waste and can be determined after evaluating serum creatinine and calculating GFR.

The most popular methods used for the analysis of creatinine are based on colorimetry or enzymatic colorimetric methods by Jaffé's reaction,[24] chromatographic methods,[25] LC-UV,[26] low-capacity cation-exchange chromatography,[27] UV/vis spectrophotometry of a copper/creatinine complex,[28] amperometric methods,[29] electrochemical impedance spectroscopy[30] and cyclic voltammetric methods.[31]

Herein, we report a Ce-complex **C1**, which was constructed from the reaction of Schiff base **L1** and cerium chloride by a hydrothermal method. Schiff base **L1** is prepared *via* the reaction of isatin with 2-amino-3-hydroxypyridin by a simple method. This complex shows strong emission at room temperature after excitation at 370 nm. Its emission is efficiently quenched by the addition of creatinine in the presence of other different interfering analytes. The molecular structures of **L1** and **C1** were theoretically studied using DFT calculations. These final data indicate that **C1** can be used as an outstanding optical biosensor for simple, fast, low-cost and highly specific and selective detection of creatinine.

Results and discussion

Characterization of Schiff base L1 and Ce(III)-complex C1

The Schiff base ligand **L1** and Ce(III) complex **C1** were prepared easily in two systems according to Scheme 1. Both **L1** and **C1** are highly colored compounds, soluble in DMSO and DMF, non-hygroscopic in nature and stable in air. The most essential physical data for the prepared compounds are provided in Table 1.

Elemental analysis

The elemental analysis of both **L1** and **C1** is presented in Table 1. The obtained results were in agreement with those calculated for the suggested formula. Anal. calc. (%): for ligand **L1**; $C_{13}H_9N_3O_2$; (239.23 g mol^{-1}); C, 65.27; H, 3.79; N, 17.56; found C, 64.95; H, 3.54; N, 16.92. And for the cerium(III)-complex **C1**; $C_{34}H_{40}CeClN_8O_9$; (880.31 g mol^{-1}); C, 46.39; H, 4.58; N, 12.73; found C, 46.62; H, 4.85; N, 12.52.

FT-IR spectra

The most significant frequencies of both **L1** and **C1** in the FT-IR spectra are presented in Fig. S1 (ESI†) and Table 1. Both spectra were in adequate agreement. **L1** exhibits a broad absorption band in the range from 3640–3300 cm^{-1}, which can be assigned to the ν(OH) of the alcohol. The band at 3120 cm^{-1} is attributed to the ν(NH) vibrations of the ring of indole. The broadband between 1754 and 2010 cm^{-1} centered at 1900 cm^{-1} can be attributed to aromatic sp^2 C–H bending patterns. The two bands at 1618 and 1704 cm^{-1} can be attributed to ν(C=O) of the isatin moiety and ν(C=N), correspondingly. The band detected at 1390 cm^{-1} is due to ν(C–N) groups. The bands at 1457 and 2930 cm^{-1} are assigned to ν(C=C) groups and ν(=C–H) groups, respectively.[32] On the other hand, the FT-IR spectrum of **C1** indicates the bonding association of the ligand with the metal ion. In contrast to the spectrum of the free ligand **L1**, in that of **C1**, we observed that there is a significant shift for the ν(OH), ν(NH), ν(C=N) and ν(C–N) vibrations. Meanwhile, the ν(C=O) and ν(C=C) vibrations stay more or less in the same place, which indicates that (C=C) does not contribute to coordination with the metal ion. Therefore, **L1** acts as a neutral bidentate coordination site *via* ν(OH), (C–N), (C=O) and azomethine nitrogen (C=N) atoms. This observation is additionally supported by new bands that were found in the 665 and 527 cm^{-1} regions assigned to ν(Ce–O) and ν(Ce–N), respectively.[33]

UV-vis spectra

The electronic absorption spectra of the ligand and its metal complex observed in DMF at room temperature are provided in Fig. S2 (ESI†). From this figure, it can be established that **L1** reveals three absorption bands at 365, 449, and 642 nm, which were assigned to intra ligand charge transfer (n–π* and π–π*). Meanwhile, **C1** reveals four absorption bands at 357, 400, 532, and 630 nm, which were assigned to ligand–metal charge transfer transitions (LMCT) and intra-ligand charge transfers (n–π* and π–π*).[34]

^{1}H-NMR spectra

The ^{1}H-NMR spectrum of the ligand **L1** (Fig. S3; ESI†) showed two signals at 10.21 and 9.58 ppm corresponding to NH and OH, respectively. The signals that appeared at 8.28, 7.29 and 7.21 ppm can be assigned to the phenyl ring protons. Benzene ring proton signals are noticed as a multiplet in the range of 6.94–7.43 ppm. The signals at 2.87 and 1.89 ppm are attributed to OH and CH_3 protons of methanol. Meanwhile, the ^{1}H-NMR spectrum of the Ce-complex **C1** (Fig. S4; ESI†) shows a signal of OH at 11.41 ppm. The signals appearing at 8.28, 7.29 and 7.21 ppm are attributed to protons of the phenyl ring, but the multiplet signals in the range of 7.77–6.94 ppm can be attributed to the protons of a benzene ring. The signals at 2.91 and 8.02 ppm conform to the CH_3 and CHO of the DMF solvent, and the signal at 2.11 ppm can be assigned to MOH.[35]

^{13}C-NMR spectra

The ^{13}C-NMR spectrum of **L1** (Fig. S5; ESI†) shows two signals at 170 and 159.6 ppm corresponding to the (C=O) and (C=N)

groups of the phenyl ring. The signals that are observed at 156 and 148.6 ppm belong to the (C=C) groups of the benzene ring, but the bands of DMSO and alcohol appeared in the range of 50–34 ppm. Meanwhile, the ^{13}C-NMR spectrum of **C1** (Fig. S6; ESI†) shows signals at 155, 140 and 138 ppm attributable to (C=O), the carbonyl group of the DMF solvent and (C=N), respectively. The signals appearing at 135 and 130 ppm belong to the phenyl ring, while the signals at 115 to 122 ppm correspond to the benzene ring. The signals appearing at 40 and 45 ppm correspond to MOH and the DMF solvent.

Mass spectra

The electron impact mass spectra of **L1** and **C1** were recorded and investigated at 70 eV of electron energy. Fig. S7 and Scheme S1 (ESI†) show the mass spectrum and the proposed fragmentation of **L1**, respectively. It is noted that the molecular ion peaks are in respectable correspondence with their suggested empirical formulae as indicated from elemental analysis. The mass spectrum fragmentation mode of the ligand demonstrates the exact mass of 239.68 (theoretically calculated was 239.23 g mol^{-1}) conforming to the formula $C_{13}H_9N_3O_2$ (Fig. S7; ESI†). The ion of m/z = 239.68 undergoes fragmentation to a stable peak at m/z = 146.22 (theoretically calculated as 146.15 g mol^{-1}) by losing C_5H_5NO atoms as shown in Scheme S1 (ESI†). The breaking of the CN bond leads to the fragmentation with m/z = 148.16. The loss of $C_2H_4N_2O$ atoms leads to the fragmentation with m/z = 78.11. The loss of NH_2 leads to the fragmentation with m/z = 57.05. A breakdown of **L1** gives the fragments in Scheme S1 (ESI†). In addition, Fig. S8 and Scheme S2 (ESI†) show the mass spectrum and the suggested fragmentation of **C1**, respectively. The mass spectrum fragmentation mode of the complex shows the exact mass of 880.54 (theoretically calculated as 880.31 g mol^{-1}) conforming to the formula $C_{34}H_{40}CeClN_8O_9$ (Fig. S8; ESI†). The ion of m/z = 880.54 undergoes fragmentation to a stable peak at m/z = 652.94 by losing two molecules of MOH and DMF and one molecule of H_2O as presented in Scheme S2 (ESI†). The loss of $C_{13}H_9N_3O_2$ atoms leads to the fragmentation with m/z = 413.79. The loss of the (Ce–Cl) bond leads to the fragmentation with m/z = 239.23. The loss of C_5H_5NO atoms leads to the fragmentation with m/z = 146.15. The loss of C_2H_3NO atoms leads to fragmentation with m/z = 93.13. A breakdown of the backbone of the complex gives the fragments in Scheme S2 (ESI†). Generally, the subsequent fragmentations of both **L1** and **C1** were inconsistent and fully agree with the molecular weight of the offered structures.

FE-SEM/EDX

The FE-SEM images and EDX analysis of **L1** and **C1** are shown in Fig. 1. **L1** in Fig. 1a and b exhibited the morphology of distributed overlapping sheets; while **C1** in Fig. 1d and e

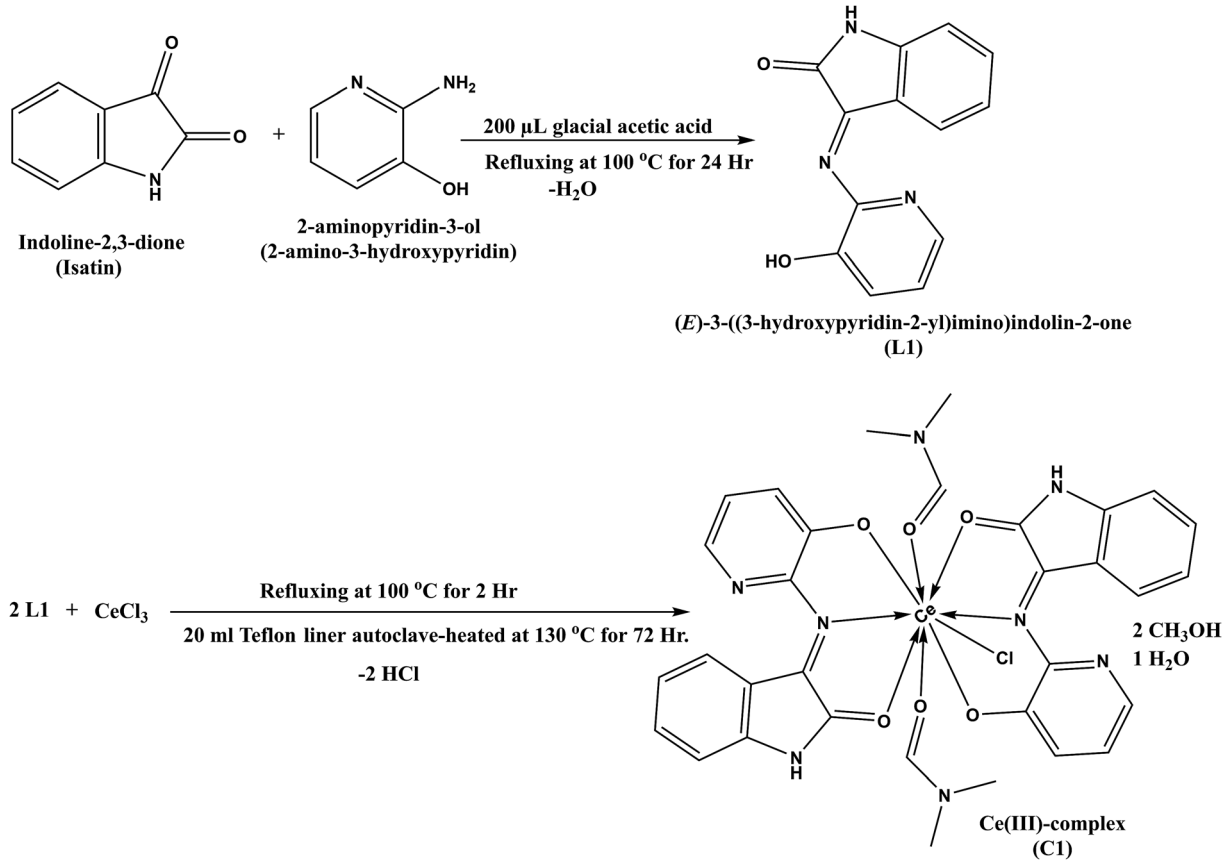

Scheme 1 The proposed scheme of the reaction of Schiff base L1, and Ce(III)-complex C1.

appeared to exhibit a macrospore shape with an average pore size of 75 nm. In addition, the EDX mapping of **L1** and **C1** is shown in Fig. 1c and f, respectively.

The EDX mapping showed the presence of carbon, nitrogen, and oxygen as the constructing block elements in **L1**, and cerium, carbon, nitrogen, chlorine, and oxygen as the constructing block elements in the distinctive particles for **C1**. Based on the beneficial results obtained and the good **L1** and **C1** distribution noticed from the SEM images, as well as the results obtained from the EDX analysis, the formation of **C1** was confirmed. Additionally, the EDX mapping confirmed our explanations and these results matched with those gained by elemental analysis and with those calculated theoretically for **L1**; C, 65.27; N, 17.56; and O, 17.17; found: C, 65.95; N, 17.57; and O, 16.48 (Table S1; ESI†); and for **C1**; C, 46.39; N, 12.73; O, 16.36; Cl, 4.03; and Ce, 15.92; found: C, 47.0; N, 13.68; O, 18.49; Cl, 4.24; and Ce, 16.59 (Table S2; ESI†).

TEM

Transmission electron microscope (TEM) images for **L1** and **C1** are presented in Fig. 2a and b, respectively. The morphology of the ligand **L1** shown in Fig. 2a was distributed overlapping sheets, while the morphology of Ce-complex **C1** shown in Fig. 2b was a well-overlapping macrospore shape. The data obtained from the TEM pattern were fairly comparable and in good correspondence with the data obtained from FE-SEM.

Based on the physical and spectral information of **L1** and **C1** discussed, we can assume that the structures of **L1** and **C1** are as suggested in Fig. 3a and b, respectively. Some representative bond distances of the optimized structures are provided in Table S3 (ESI†). In addition, the cartesian coordinates of the optimized structures are provided in Tables S4 and S5 (ESI†).

Theoretical and computational methods

Geometry optimizations and other DFT calculations were performed on the Schiff base **L1** and its cerium(III) complex **C1**. DFT is considered a cost-effective method to approximate electron correlation effects. All DFT calculations were performed by using the B3LYP level of theory, Becke's three parameter (B3) nonlocal exchange with the correlation functional of Lee, Yang, and Parr (LYP).[36] Nowadays, the B3LYP level is currently widely used to study organic electronic compounds because the predicted geometries are very reliable and provide good estimations for the HOMO–LUMO gaps, in good agreement with experimental values. All of the calculations were carried out at the B3LYP/6-31g(d) level for all atoms, except Ce atoms were described by using the CEP-4g basis set.[37] All computations were carried out by using the Gaussian09 suite of programs.[38] The Gauss View 5.0 package was used to obtain various graphic views of molecular shapes of distinctive molecular orbitals.

DFT calculations

The major elements of augmented geometry of the Ce(III) complex seem to have an octahedral geometry, Fig. 3b. The highest occupied molecular orbitals (HOMOs) and lowest unoccupied molecular orbitals (LUMOs) are actual substantial elements of the theoretical molecular sketch.[39] Fig. 4 represents the HOMO and LUMO of **L1** and **C1**; the HOMO is the donor site for the electrons and the LUMO is the acceptor site of the electrons. The molecular softness and hardness of any compound can be expected from the gap between the HOMO and LUMO.[40] Soft molecules have a small energy gap (E_g), whereas hard molecules have enormous (E_g) values.[41,42]

Table 1 Analytical and some important physical measurements for L1 and C1

Assignments		L1	C1
Preparation method		Reflux	Hydrothermal
Color		Light green	Dark green
Aspect		Powder	Fine crystal
Melting point (°C)		113	>300
Reaction time		1 days	3 days
Yield (%)		78.0	70.8
Chemical formula		$C_{13}H_9N_3O_2$	$C_{34}H_{40}CeClN_8O_9$
Molecular weight (g mol^{-1})		239.23	880.31
Elemental analysis (calc.)/found	C%	(65.27)/64.95	(46.39)/46.62
	H%	(3.79)/3.54	(4.58)/4.85
	N%	(17.56)/16.92	(12.73)/12.52
Characteristic infrared frequencies (cm^{-1})	ν(OH)	3640–3300	3675–3250
	ν(NH)	3120	3062
	ν(C=O)	1618	1621
	ν(C=N)	1704	1712
	ν(C–N)	1390	1353
	ν(C=C)	1457	1465
	ν(C–H)	2930	2779
	ν(Ce–O)	—	665
	ν(Ce–N)	—	527
UV-λ_{max} (nm)		365, 449, 642	357, 400, 532, 630

From the calculations of E_g, **C1** was found to be more reactive than **L1**. The charge separation (polarity) over the molecule, which is calculated from the dipole moment (μ), illustrates that the μ of **C1** is higher than the μ of **L1** ($\mu_{C1} > \mu_{L1}$). Moreover, it was noticed that there is a transfer of charge density from **L1** atoms to the metal ion (Ce). In addition, there is a back-donation of electrons from the cerium ion to the Schiff base donating atoms after the complexation process. The greater reactivity of **C1** over **L1** is described by the difference in E_g, which determines the reactivity; as the E_g increases, the reactivity decreases and hence the quantity of electronic charge transfer from **L1** to **C1** (central cerium metal ion) increases. The E_{HOMO}, E_{LUMO}, E_g, and μ of **L1** and **C1** are recorded in Table 2.

Photoluminescence study and applications

The photoluminescence of Ce-complex **C1** was reported at different wavelengths of excitation as revealed in Fig. 5a. To establish the optimal wavelength for photoluminescent excitation, excitation spectra were first obtained by measuring emission at the maximum intensity wavelength. From Fig. 5a it was realized that **C1** had a high emission peak at 560 nm after excitation at 370 nm. The excitation and emission spectra of **C1** are shown in Fig. 5b.

Using the Ce(III)-complex as an optical sensor for creatinine

The PL spectra of **C1** (1×10^{-3} M in distilled water solutions) were examined *versus* various concentrations of creatinine (Fig. 5c). From Fig. 5c, the PL intensities of **C1** were highly quenched as the creatinine concentration increased.

Calibration curve and detection limit

The linear correlation graph between the PL intensity of **C1** at λ_{em} = 560 nm after excitation at λ_{ex} = 370 nm and the creatinine concentration in the range between 2.5 nM to 480 nM is presented in Fig. 5d, and a summary of the regression analysis data is provided in Table S6 (ESI†). The LOD was found to be 1.07 nM, whereas the LOQ was 3.25 nM, with a dynamic line range of 2.5–480 nM. The low LOD value was considered as verification of the extreme sensitivity of the applied approach. The contrast between the analytical performance of the current work and other published methods[26–31] for creatinine determination is presented in Table 3. From the comparison evaluation, it can be noted that this method exhibited a fast response time, high sensitivity, high accuracy and precision, good reproducibility, applicability, good recovery and effectiveness, a wider linear range and lower values of LOD and LOQ in comparison with other reports. Also, many of the published methods are more costly, more time-consuming and carried out in several steps.

Selectivity and interference study

The selectivity of the applied optical biosensor based on **C1** to creatinine was investigated by observing the impact of the presence of other interfering analytes on the **C1** PL intensity as

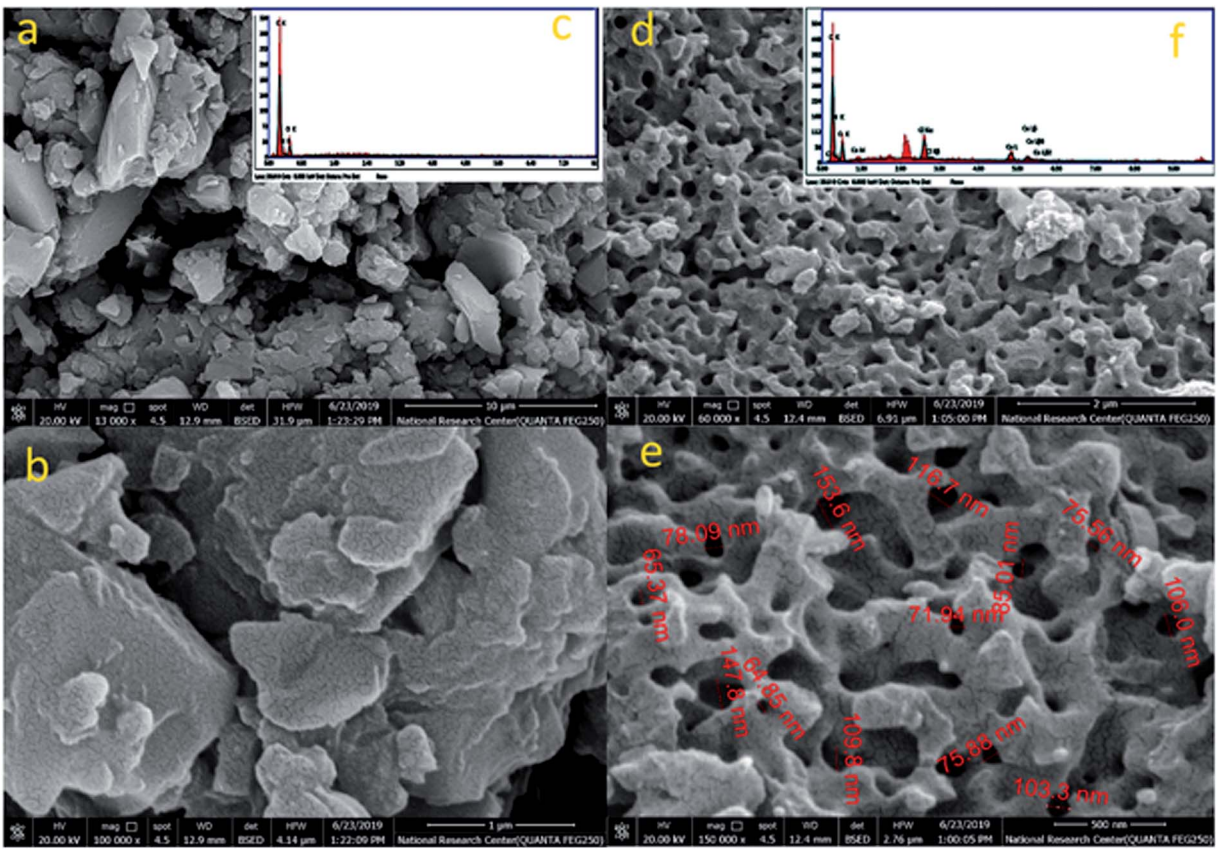

Fig. 1 SEM and EDX images: [a–c] Schiff base **L1**, and [d–f] Ce(III)-complex **C1**.

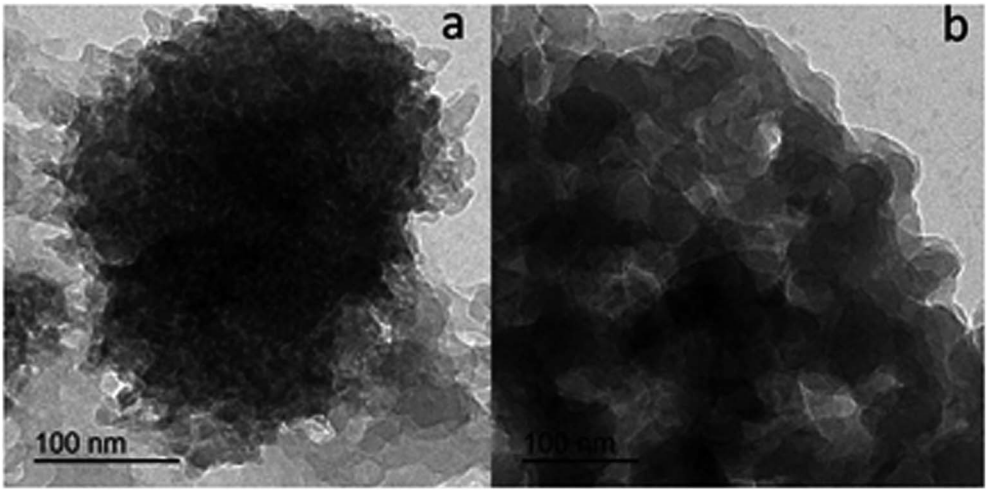

Fig. 2 TEM image of: [a] Schiff base **L1**, and [b] Ce(III)-complex **C1**.

shown in Fig. 5e and S9 (ESI†). The PL spectra of **C1** (1×10^{-3} M) against different interfering analytes in distilled water solutions [uric acid 6.0 mg dL^{-1}, ascorbic acid 0.5 mg dL^{-1}, glycine 0.5 μM mL^{-1}, acetaminophen 100 mg mL^{-1}, glucose 100 mg dL^{-1}, and creatinine 100 nM] were considered. From these figures, the intensity of the PL spectrum of **C1** isn't affected by these various kinds of interfering analytes. This indicates that **C1** is extremely sensitive and enormously selective for creatinine due to the enormous quenching effect even in the presence of numerous competing interfering analytes. The PL quenching histogram of **C1** upon the series addition of creatinine with different concentrations is shown in Fig. S10 (ESI†).

Accuracy and precision

The accuracy and the precision of the currently suggested biosensor for creatinine determination were assessed and a summary of the obtained information is provided in Table S7 (ESI†). The present investigation was done at four creatinine concentrations (5.0, 50.0, 100.0, and 250.0 nM). The process of measurement was recorded (3) times on various days and on the same day to examine the reproducibility and repeatability of our work. Based on the obtained table of data: the mean values (X) were 5.033, 48.67, 99.5, and 241.3 nM, with an average standard deviation (SD) of 0.208–2.165, and a coefficient of variation (CV) of 0.043–4.688, for intra-day measurements. In addition, X was 4.831, 49.22, 99.18, and 251.7 nM, with SD of 0.235–3.25, and CV of 0.055–3.58, for inter-day measurements. The proximity of the investigated data from the X values and the lower values of SD as well as the CV values demonstrate the extraordinary precision of this approach. Furthermore, the analyzed obtained values for the relative-error percent (RE%) for inter/intra-day measurements, which were ≤1.04%, indicate the high accuracy of the suggested creatinine biosensor.

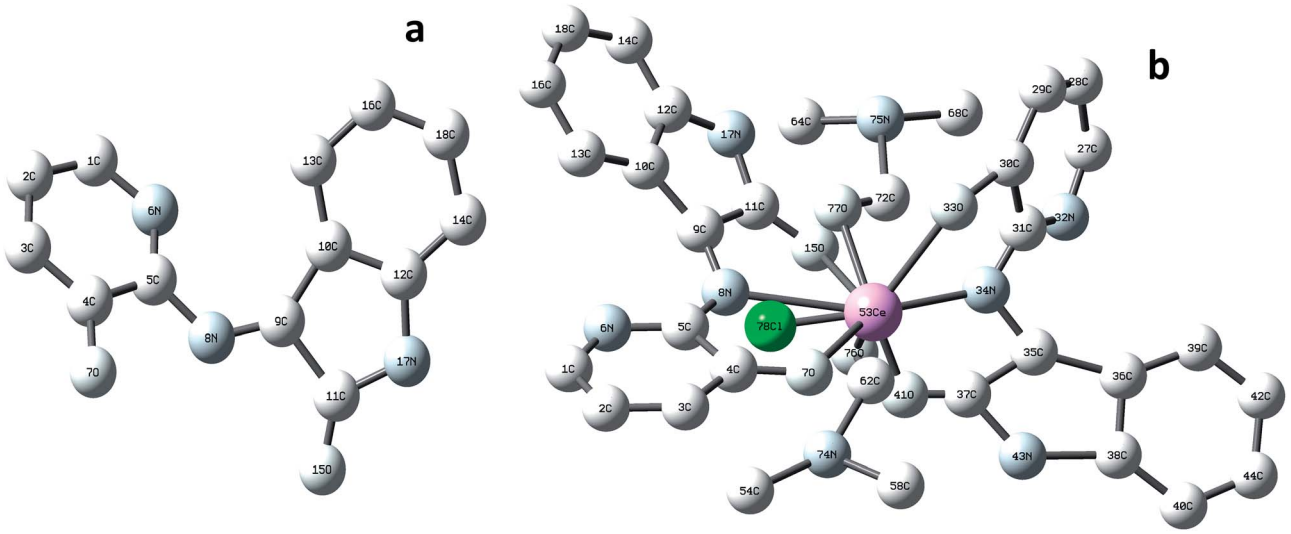

Fig. 3 Optimized structures of [a] Schiff base **L1**, and [b] Ce(III)-complex **C1**.

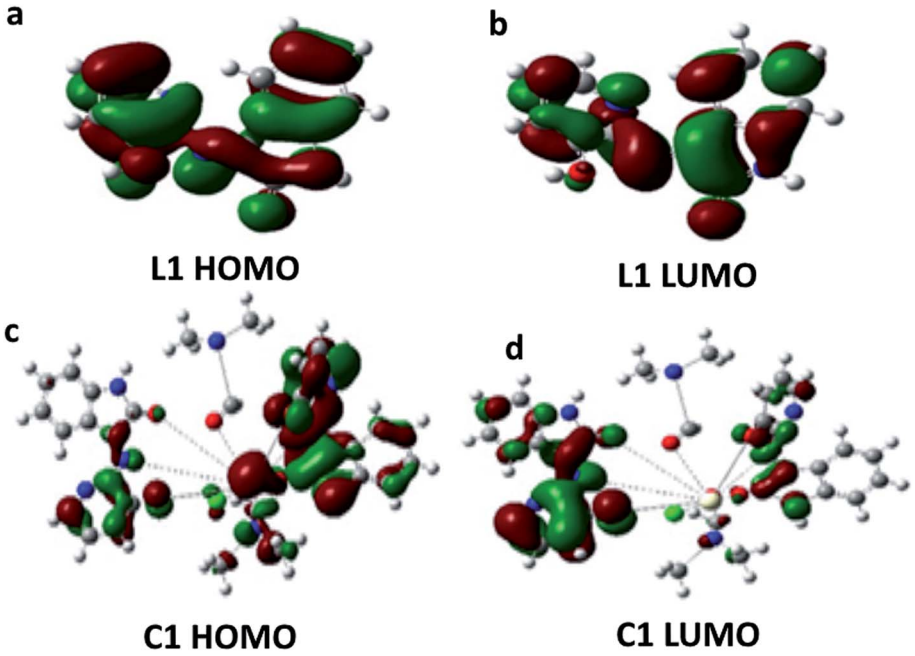

Fig. 4 HOMO and LUMO energy level images of: [a and b] Schiff base **L1**, and [c and d] Ce(III)-complex **C1**.

Application to real samples & recovery study

The current investigation was accomplished to examine the effectiveness, ability, and applicability of **C1** to confirm creatinine in various real samples (serum and plasma). The investigation was done by spiking serum or plasma samples with creatinine standard at various concentrations (50.0, 100.0 and 200.0 nM), performing each experiment 3 times, and then the suggested method was applied to determine their creatinine content. The data obtained from the recovery (RE) investigation, including the relative standard deviation (RSD), are provided in Table S8 (ESI†). The results in Table S8† show that the recovery values (percent ± SD) of creatinine were 101.3 ± 2.02, 97.42 ± 1.34, and 98.34 ± 0.40 for the serum samples, and 98.34 ± 0.10, 98.49 ± 2.70, and 97.55 ± 2.94 for the plasma samples. Hence, the nearness of RE values to one hundred percent and the lower RSD values (less than 2.94%) together demonstrate that the current method has a quite respectable accuracy and that the current suggested method can be applied for the determination of creatinine with acceptable results.

Mechanism of PL quenching

The mechanism of interaction and quenching between the sensing material (Ce-complex) and the quencher (creatinine), was determined by studying the quenching in the PL band intensities of **C1** upon systematic addition of creatinine as shown in Fig. 5c.[43,44] Herein, the Ce-complex acts as the electron donor site and creatinine acts as the electron acceptor site. The lanthanide luminescence behavior is due to the 4f–5d transition rather than the conventional 4f–4f transition, which means that Ce(III) complexes can be used as electroluminescent devices.[45] The emission wavelengths can be adjusted by using suitable ligands,[46] so the photocatalytic properties of the cerium(III) complexes are due to their outer-sphere electrons, as observed for homoleptic tris-guanidinate.[47] Herein, the variation in the PL intensity of **C1** with increasing creatinine concentration occurs due to the interaction between **C1** and creatinine. The observed PL quenching is expected to be due to the electron or energy transfer between the donor site **C1** and acceptor site (creatinine) or it may be due to the fast quenching of the excited state of Ce(III), which results from non-radiative relaxation pathways.[48] The energy transfer from the excited state of **C1** (as a donor site) to creatinine (as an acceptor site) through non-radiative dipole–dipole coupling is the basic possible mechanism.[49] Furthermore, the FRET mechanism can be described as the quenching mechanism if the distance (R^o) (critical radius/critical transfer distance) between the donor **C1** and acceptor (creatinine) is lower than 10 Å. By using the Stern–Völmer equation on the acquired results and from the linear calibration graph in Fig. 5d:

$$K_{sv}\text{ value} = 0.01549;\ C^o = 1/K_{sv} = 64.558;\ R^o = 7.35C^{o-1/3};$$
$$R^o = 7.35 \times (64.558)^{-1/3};\ R^o = 1.83\ \text{Å}.$$

Table 2 The energy of the HOMO (eV), the energy of the LUMO (eV), the energy gap (eV) and the dipole moment (Debye) for the Schiff base **L1** and Ce(III)-complex **C1**

Parameter	L1	C1
E_{HOMO} (eV)	−5.81	−4.85
E_{LUMO} (eV)	−2.29	−2.97
E_{gap} (eV)	3.52	1.88
μ (D)	4.42	4.84

where C^{o} is the critical value of creatinine concentration, and R^{o} is the distance between creatinine and **C1**. Hence, the R^{o} was 1.83 Å from the above calculations and so we can conclude that the quenching mechanism is due to the energy transfer between the **C1** and creatinine.[50,51]

Furthermore, a temperature dependence investigation can determine or predict the quenching mechanism category for any system that may be a dynamic or static mechanism. In the case of a dynamic mechanism, the value of K_{sv} increases as the temperature increases, and for the static mechanism type, the value of K_{sv} decreased as the temperature increased. The Stern–Völmer graph of the PL quenching of **C1** with diverse concentrations of creatinine at several temperatures (298, 300, 303, and 308 K) was plotted. As shown in the Stern–Völmer plot in Fig. 5f, the plot presents effective linearity within the studied concentrations of creatinine. In addition, it was established that the slopes (K_{sv} values) of the **C1** plots were directly proportional to the temperature (Table S9, ESI†), which proves that the quenching mechanism between **C1** and creatinine is dynamic.[43,52]

Experimental

Materials

All solvents and chemicals used in this study are analytical reagent grade and were used as received. Isatin ($C_{11}H_{10}$), 2-

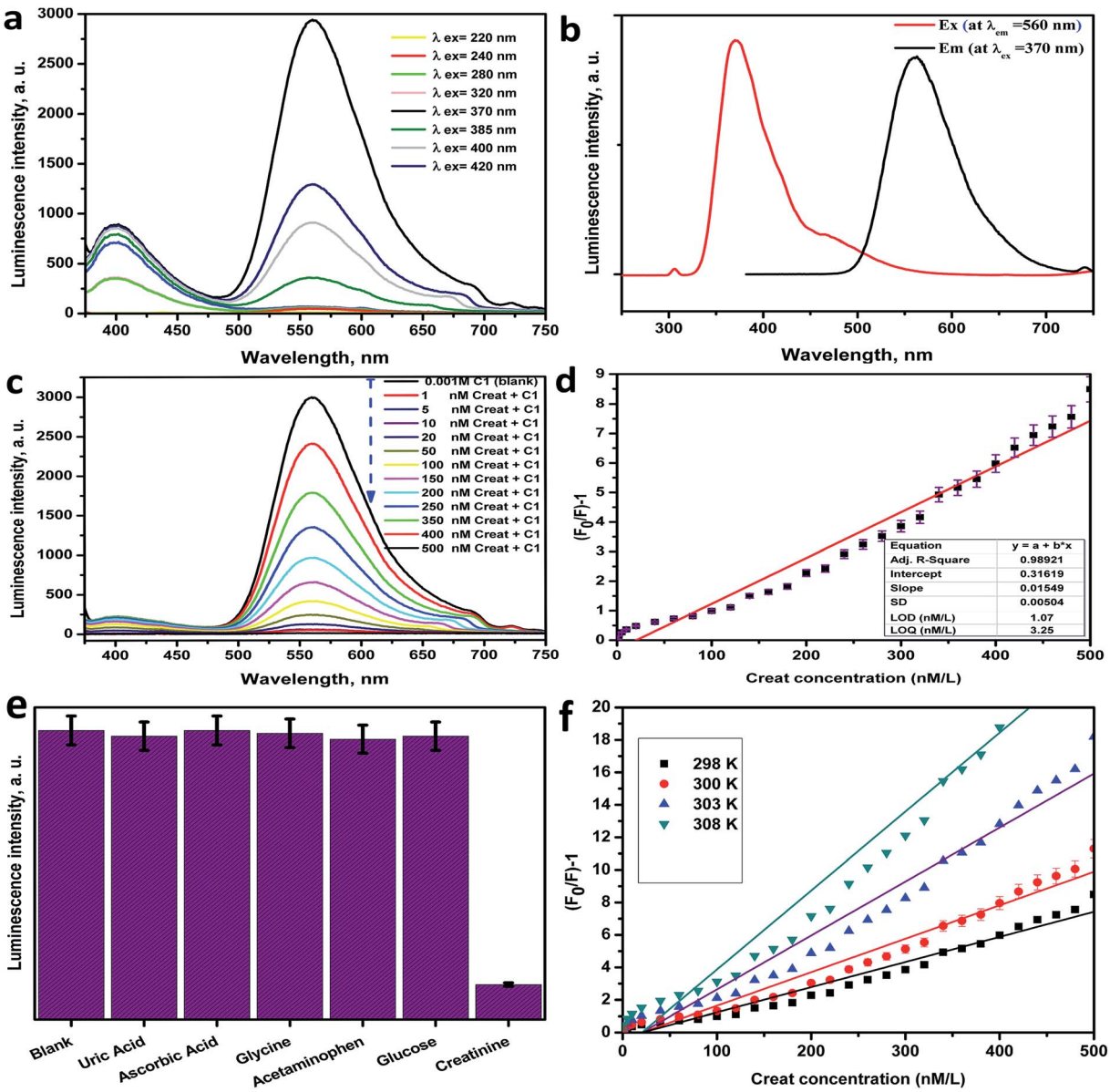

Fig. 5 [a] The PL emission spectra at different excitation wavelengths for **C1**. [b] Excitation (red line) and emission (black line) spectra of **C1**. [c] The PL spectra showing the behavior of **C1** towards human creatinine. [d] The linear relationship between the photoluminescence intensity of **C1** and different concentrations of human creatinine. [e] The PL enhancement efficiency histogram of **C1** against different types of interferents. [f] The Stern–Völmer plots for PL quenching of **C1** by creatinine at four different temperatures.

amino-3-hydroxypyridin ($C_5H_6N_2O$) and cerium(III)chloride anhydrous $CeCl_3$; 99.9% were purchased from Sigma-Aldrich.

Instruments

The characterization was carried out using different analytical equipment: the field emission scanning electron microscopy (FE-SEM) images and element mapping by spatially resolved energy dispersive X-ray spectroscopy (EDX) were recorded with a JEOL JSM-6510LV advanced electron microscope with a LAB-6 cathode at 520 keV (JEOL, Japan). The structure of the formed phases was examined by using a high-resolution transmission electron microscope (HR-TEM) with an acceleration voltage up to 200 kV (TEM, JEOL-JEM-2100, Tokyo, Japan). Fourier transform infrared (FT-IR) spectra were recorded on a JASCO FT/IR-460 spectrophotometer using KBr tablets, at room temperature in the range 400–4000 cm^{-1} (JASCO, USA). Ultra violet-visible (UV-vis) spectra were obtained for the prepared Schiff base ligand (HL) and metal complex by using a PerkinElmer 550 spectrophotometer in a 1 cm quartz cell in ethanol, over a range of 200–900 nm. Mass spectra of the solid ligand and complex were registered using a Thermo Scientific, ISQ Single Quadrupole MS (Thermo Scientific, USA). ^{1}H-NMR and the ^{13}C-NMR spectra were acquired in DMSO-d_6 using a Gemini-300 MHz NMR spectrometer (ECA 500 II, JEOL, Japan). Elemental analysis (C, H, and N) was achieved using a Costech (ECS-4010) elemental analyzer (Costech, Italy). The photoluminescence (PL) emission spectra were obtained using a spectrofluorophotometer (Shimadzu RF-5301PC, Japan). The samples were investigated at room temperature at a different excitation wavelength and the data analysis was executed by Origin (8) software.

Procedure

Synthesis of (*E*)-2-((3-hydroxypyridin-2-yl)imino)indolin-3-one (L1). Schiff base was prepared as follows: isatin (1 mmol, 1.471 g) was dissolved in 30 mL methanol/10 mL DMF and was added to a solution of 2-amino-3-hydroxypyridin (1 mmol, 1.101 g) dissolved in methanol (10 mL) in the presence of four drops of glacial acetic acid (about 200 μL). The resulting mixture was refluxed for 24 hours at 100 °C in a closed system. The mixture was left to cool, and the precipitated Schiff base was light green (Scheme 1). The collected precipitate was washed with 20 mL distilled water and 20 mL acetone, and then dried at 100 °C, the calculated yield was 78.0%.

Synthesis of cerium(III) complex C1. Cerium chloride anhydrous $CeCl_3$ (1 mmol, 1.232 g) was dissolved in 10 mL distilled water, and then added to 2 mmol Schiff base **L1** as shown in Scheme 1. This system was refluxed for 2 hours, and then the mixture was shifted to an autoclave for 72 hours and heated at 130 °C. After cooling the mixture at room temperature, the precipitate was dark green (Scheme 1). The resulting precipitate was washed with 20 mL of distilled water and then with acetone and dried, and the calculated yield was 70.8%.

Computational methods. The geometry optimizations and all DFT calculations on the Schiff base **L1** and its cerium(III) complex **C1** were performed using the Gaussian09 suite of programs.[38]

Photoluminescence study and applications. The Ce(III) complex used in the present study was obtained from a stock solution of **C1** dissolved in dimethyl sulfoxide (1×10^{-2} M) and was added to a clean 10 mL measuring flask, and then appropriate concentrations (1×10^{-9} to 1×10^{-3} M) were obtained by dilution to the mark with distilled water. These solutions were used for the subsequent photoluminescence measurements. The photoluminescence intensities were measured at different excitation wavelengths at room temperature. The photoluminescence spectra of **C1** (1×10^{-3} M) in a distilled water solution with different analytes were recorded for selected excitation wavelengths.

To determine creatinine using the Ce(III) complex, the PL spectra of **C1** (1×10^{-3} M) in distilled water against different concentrations of standard creatinine as described above were recorded. The required concentrations were recently prepared before the measurement step. Also, each concentration was done in a separate step to avoid the carry-over and/or adsorption of this concentration of creatinine on the sample container or cuvette and then the samples were determined at the chosen excitation wavelength. A linear relationship was established between the photoluminescence intensity of Ce-complex **C1** at $\lambda_{em} = 560$ nm and the creatinine concentration in the range between 2.5 and 480 nM. The graph was expressed *via* a regression equation: $Y = a + bX$ where Y = photoluminescence intensity of **C1** at $\lambda_{em} = 560$ nm; a = intercept; b = slope and X = concentration of creatinine in nM. The regression data analysis of photoluminescence intensity was carried out by applying the least-squares method to evaluate the slope, intercept and correlation coefficient (r^2) values. The LOD and LOQ were calculated from the equations: LOD = $3.3S/b$ and LOQ = $10S/b$[53]

Table 3 Comparison of the photoluminescence approach with some existing methods for the determination of creatinine

Method	Linear range (μM)	Limit of detection (μM)	Reference
LC-UV method	20–900	~1.5	26
Low-capacity cation-exchange chromatography	1–1000	0.02	27
UV/vis spectrophotometry of a copper/creatinine complex	8.8–530	2.5	28
Amperometric detection	10–650	0.5	29
Electrochemical impedance spectroscopy	0.05–0.2 μg mL^{-1}	~0.35	30
Cyclic voltammetry	10	0.001	31
Photoluminescence approach	2.5–480 nM	1.07 nM	Present work

where S is the blank standard deviation of the photoluminescence intensity values, and b is the slope of the calibration graph.

Determination of creatinine in real samples. Real serum samples from healthy females and males were supplied from a medical laboratory. Then, blood samples were collected by jugular venipuncture in test tubes and centrifuged immediately for 15 min at 4000 rpm min^{-1}. The obtained serum samples were stored at −20 °C until being assayed for creatinine. The procedure of the PL measurements described above was applied to study the effect of creatinine in the serum samples upon appropriate dilution of the spiked samples (spiking techniques). The measured PL intensities were introduced into the linear portion of the constructed calibration graph obtained with creatinine standard solutions.

Conclusions

A novel optical creatinine approach was suggested by the preparation of a smart sensing material [Ce(III)–isatin Schiff base complex]. The current optical sensor (**C1**) exhibited fast response time, high sensitivity, high accuracy and precision, good reproducibility, applicability, good recovery and effectiveness to determine creatinine in various real samples (serum/plasma). This study supplies a suitable approach to develop a new kind of creatinine biosensor with an enormous linear range and lower LOD and LOQ values compared with other published reports. The nature of the interaction and quenching mechanism was also well investigated by using the Stern–Völmer equation. The results of this study indicated that the energy-transfer was responsible for the quenching of our system and the quenching mechanism between **C1** and creatinine was a dynamic type. DFT calculations were executed to investigate the optimized structures of **L1** and **C1**.

Statement of human and animal rights

The human patient samples used in this study were provided by the Family Medical Laboratory, Ministry of Health, Cairo, Egypt. Informed consent was obtained. The studies were approved by the appropriate ethics committee (Ministry of Health, Egypt) and were performed in accordance with ethical standards of the responsible committee on human experimentation (institutional and national) and with the Helsinki Declaration of 1975, as revised in 2000 and 2008 ethical standards. We did not use the samples in any research involving human participants or research involving physical interventions on study participants or involving processing of personal data but conducted the research according to the method described in the article.

Conflicts of interest

There are no conflicts to declare.

Notes and references

1 D. R. Smith, J. B. Pendry and M. C. K. Wiltshire, *Science*, 2004, **305**, 788–792.
2 D. Ghosh, P. Karmakar, K. Biswas, S. Balaji, A. D. Sontakke and K. Annapurna, *Phys. Chem. Glasses: Eur. J. Glass Sci. Technol., Part B*, 2014, **55**, 196–206.
3 J. Tang, L. Zhou, W. Wang, C. Yang, J. H. Zhou and Y. H. Zhou, *J. Lumin.*, 2012, **132**, 1325–1328.
4 M. Abdelaziz, *Phys. B Condens. Matter*, 2011, **406**, 1300–1307.
5 B.-I. Wu, W. Wang, J. Pacheco, X. Chen, T. Grzegorczyk and J. A. Kong, *Prog. Electromagn. Res.*, 2005, **51**, 295–328.
6 A. Vora, J. Gwamuri, N. Pala, A. Kulkarni, J. M. Pearce and D. O. Guney, *Sci. Rep.*, 2014, **4901**, 1–13.
7 D. Schurig, J. J. Mock, B. J. Justice, S. A. Cummer, J. B. Pendry, A. F. Starr and D. R. Smith, *Science*, 2006, **314**, 977–980.
8 H. Kunkely and A. Vogler, *J. Photochem. Photobiol., A*, 2002, **151**, 45–47.
9 H. Yin, P. J. Carroll and E. J. Schelter, *Inorg. Chem.*, 2016, **55**, 5684–5692.
10 A. Vogler and H. Kunkely, *Inorg. Chim. Acta*, 2006, **359**, 4130–4138.
11 Y. Hasegawa, Y. Kimura, K. Murakoshi, Y. Wada, J. H. Kim, N. Nakashima, T. Yamanaka and S. Yanagida, *J. Phys. Chem.*, 1996, **100**, 10201–10205.
12 X. L. Zheng, Y. Liu, M. Pan, X. Q. Lü, J. Y. Zhang, C. Y. Zhao, Y. X. Tong and C. Y. Su, *Angew. Chem., Int. Ed.*, 2007, **46**, 7399–7403.
13 A. D. Garnovskii, A. L. Nivorozhkin and V. I. Minkin, *Coord. Chem. Rev.*, 1993, **126**, 1–69.
14 S. K. Sridhar, S. N. Pandeya and E. De Clercq, *Boll. Chim. Farm.*, 2001, **140**, 302–305.
15 B. Thadhaney, D. Sain, G. Pemawat and G. L. Talesara, *Indian J. Chem.*, 2010, **49B**, 368–373.
16 R. S. Varma and W. L. Nobles, *J. Pharm. Sci.*, 1975, **64**, 881–882.
17 S. N. Pandeya, D. Sriram, G. Nath and E. De Clercq, *Eur. J. Med. Chem.*, 2000, **35**, 249–255.
18 J. C. Logan, M. P. Fox, J. H. Morgan, A. M. Makohon and C. J. Pfau, *J. Gen. Virol.*, 1975, **28**, 271–283.
19 S. C. Kazmierczak, F. Van Lente and E. D. Hodges, *Clin. Chem.*, 1991, **37**, 356–360.
20 S. Narayanan and H. Appleton, *Clin. Chem.*, 1980, **26**, 1119.
21 L. C. Chesley, *J. Clin. Invest.*, 2008, **17**, 591–597.
22 R. Cánovas, M. Cuartero and G. A. Crespo, *Biosens. Bioelectron.*, 2019, **130**, 110–124.
23 H. Strevens, D. Wide-Swensson and A. Grubb, *Scand. J. Clin. Lab. Invest.*, 2001, **61**, 575–580.
24 J. A. Weber and A. P. Van Zanten, *Clin. Chem.*, 1991, **37**, 695–700.
25 C. J. Kochansky and T. G. Strein, *J. Chromatogr. B: Biomed. Sci. Appl.*, 2000, **747**, 217–227.
26 A. K. Dash and A. Sawhney, *J. Pharm. Biomed. Anal.*, 2002, **29**, 939–945.

27 Y. Yokoyama, S. Tsuji and H. Sato, *J. Chromatogr. A*, 2005, **1085**, 110–116.
28 P. Nagaraja, K. Avinash, A. Shivakumar and H. Krishna, *Spectrochim. Acta, Part A*, 2012, **92**, 318–324.
29 S. Yadav, R. Devi, A. Kumar and C. S. Pundir, *Biosens. Bioelectron.*, 2011, **28**, 64–70.
30 B. Khadro, A. Betatache, C. Sanglar, A. Bonhommé, A. Errachid and N. Jaffrezic-Renault, *Sens. Lett.*, 2011, **9**, 2261–2264.
31 M. D. Guo, H. T. Liu and Y. Li, *Chin. J. Anal. Chem.*, 1999, **244**, 475–478.
32 K. Nakamoto, in *Handb. Vib. Spectrosc.*, ed. P. R. Griffiths, John Wiley & Sons, Ltd, Chichester, UK, 2006.
33 M. Shebl, M. A. Ibrahim, S. M. E. Khalil, S. L. Stefan and H. Habib, *Spectrochim. Acta, Part A*, 2013, **115**, 399–408.
34 F. Zhang, H. Yao, T. Chu, G. Zhang, Y. Wang and Y. Yang, *Chem.–Eur. J.*, 2017, **23**, 10293–10300.
35 S. M. Sheta, S. M. El-Sheikh, M. M. Abd-Elzaher, M. L. Ghanem and S. R. Salem, *RSC Adv.*, 2019, **9**, 20463–20471.
36 A. D. Becke, *J. Chem. Phys.*, 1993, **98**, 5648–5652.
37 T. R. Cundari and W. J. Stevens, *J. Chem. Phys.*, 1993, **98**, 5555–5565.
38 M. J. Frisch, G. W. Trucks, H. B. Schlegel, G. E. Scuseria, M. A. Robb, J. R. Cheeseman, G. Scalmani, V. Barone, B. Mennucci, G. A. Petersson, H. Nakatsuji, M. Caricato, X. Li, H. P. Hratchian, A. F. Izmaylov, J. Bloino, G. Zheng, J. L. Sonnenberg, M. Had, M. Ehara, K. Toyota, R. Fukuda, J. Hasegawa, M. Ishida, T. Nakajima, Y. Honda, O. Kitao, H. Nakai, T. Vreven, J. A. Montgomery, Jr, J. E. Peralta, F. Ogliaro, M. Bearpark, J. J. Heyd, E. Brothers, K. N. Kudin, V. N. Staroverov, T. Keith, R. Kobayashi, J. Normand, K. Raghavachari, A. Rendell, J. C. Burant, S. S. Iyengar, J. Tomasi, M. Cossi, N. Rega, J. M. Millam, M. Klene, J. E. Knox, J. B. Cross, V. Bakken, C. Adamo, J. Jaramillo, R. Gomperts, R. E. Stratmann, O. Yazyev, A. J. Austin, R. Cammi, C. Pomelli, J. W. Ochterski, R. L. Martin, K. Morokuma, V. G. Zakrzewski, G. A. Voth, P. Salvador, J. J. Dannenberg, S. Dapprich, A. D. Daniels, O. Farkas, J. B. Foresman, J. V. Ortiz, J. Cioslowski and D. J. Fox, Gaussian, Inc., Wallingford CT.
39 D. Shoba, S. Periandy, M. Karabacak and S. Ramalingam, *Spectrochim. Acta, Part A*, 2011, **83**, 540–552.
40 K. Fukui, *Science*, 1982, **218**, 747–754.
41 R. G. Pearson, *Chemical Hardness*, 2005, **26**, 99–124.
42 A. E. Reed, L. A. Curtiss and F. Weinhold, *Chem. Rev.*, 1988, **88**, 899–926.
43 S. M. Sheta, S. M. El-Sheikh, M. M. Abd-Elzaher and A. R. Wassel, *Appl. Organomet. Chem.*, 2019, **33**, e4777.
44 S. M. Sheta, S. M. El-Sheikh and M. M. Abd-Elzaher, *Appl. Organomet. Chem.*, 2019, **33**, e5069.
45 P. N. Hazin, J. W. Bruno and H. G. Brittain, *Organometallics*, 1987, **6**, 913–918.
46 H. Yin, P. J. Carroll, J. M. Anna and E. J. Schelter, *J. Am. Chem. Soc.*, 2015, **137**, 9234–9237.
47 D. M. Schultz and T. P. Yoon, *Science*, 2014, **343**, 1239176.
48 S. Cotton, *Lanthanide and Actinide Chemistry*, John Wiley & Sons, Ltd, UK, 2006.
49 J. R. Lakowicz, *Principles of Fluorescence Spectroscopy*, Springer US, New York, United States 2006.
50 L. S. Walekar, S. P. Pawar, U. R. Kondekar, D. B. Gunjal, P. V. Anbhule, S. R. Patil and G. B. Kolekar, *J. Fluoresc.*, 2015, **25**, 1085–1093.
51 Y.-Z. Zhang, B. Zhou, Y.-X. Liu, C.-X. Zhou, X.-L. Ding and Y. Liu, *J. Fluoresc.*, 2008, **18**, 109–118.
52 S. M. Sheta, S. M. El-Sheikh and M. M. Abd-Elzaher, *Anal. Bioanal. Chem.*, 2019, **411**, 1339–1349.
53 M. M. Abd-Elzaher, M. A. Ahmed, A. B. Farag, M. S. Attia, A. O. Youssef and S. M. Sheta, *Sens. Lett.*, 2017, **15**, 977–981.